ChemPubSoc Europe

DOI: 10.1002/chem.201605685

CHEMISTRY A European Journal Full Paper

Heterogeneous Catalysis

TNU-9 Zeolite: Aluminum Distribution and Extra-Framework Sites of Divalent Cations

Robert Karcz,[a, b] Jiri Dedecek,[a] Barbara Supronowicz,[a] Haunani M. Thomas,[a] Petr Klein,[a] Edyta Tabor,[a] Petr Sazama,[a] Veronika Pashkova,[a] and Stepan Sklenak*[a]

Abstract: The TNU-9 zeolite (TUN framework) is one of the most complex zeolites known. It represents a highly promising matrix for both acid and redox catalytic reactions. We present here a newly developed approach involving the use of ^{29}Si and ^{27}Al (3Q) MAS NMR spectroscopy, Co^{II} as probes monitored by UV/Vis and FTIR spectroscopy, and extensive periodic DFT calculations, including molecular dynamics, to investigating the aluminum distribution in the TUN framework and the location of aluminum pairs and divalent cations in extra-framework cationic positions. Our study reveals that 40 and 60% of aluminum atoms in the TNU-9 zeolite are isolated single aluminum atoms and aluminum pairs, respectively. The aluminum pairs are present in two types of six-membered rings forming the corresponding α and β (15 and 85%, respectively, of aluminum pairs) sites of bare divalent cations. The α site is located on the TUN straight channel wall and it connects two channel intersections. The suggested near-planar β site is present at the channel intersection.

Introduction

Zeolites are crystalline aluminosilicates with frameworks composed of corner-sharing TO_4 tetrahedra (T = Si, Al^-). The variability of arrangements of TO_4 tetrahedra results in more than 200 known zeolite topologies with different microporous channel and cavity systems.[1] Framework Al/Si substitutions introduce a negative charge that is compensated by protons, metal cations, and metal–oxo cations. These exchangeable, positively charged extra-framework species can act as catalytic and sorption centers. The unique properties of the cationic species together with the variability of the zeolite channel systems are responsible for the fact that zeolites represent a wide and very important group of heterogeneous catalysts.[2]

The organization of aluminum atoms in the framework of silicon-rich zeolite catalysts is a key property.[2] The aluminum organization includes the aluminum siting (i.e., which different distinguishable framework T sites are occupied by isolated single aluminum atoms), aluminum distribution (i.e., the distribution of framework aluminum atoms between Al-O-(Si-O)$_2$-Al sequences in the rings forming cationic sites for divalent cations and isolated single aluminum atoms),[3] and the location of framework aluminum atoms in the channel system of the zeolite, which can be in either the channels or at the channel intersections.[4] The positively charged active species balance the negative charge of AlO_4^- tetrahedra, and therefore, the organization of aluminum atoms in the zeolite framework controls the formation and properties of active sites in the zeolite.[2,4,5] The aluminum siting determines the location of the active sites in the zeolite framework whereas the aluminum distribution controls the concentration and stability of mono- and divalent cations and metal–oxo species.[2,3,6] In addition, for monovalent cationic species, including protons, the aluminum distribution also controls the distance between the active sites and thus a possibility of their cooperation.[7] Several catalytic studies have shown that zeolites of the same chemical composition but different aluminum organization could possess different catalytic properties.[2] Thus, the potential of a zeolite for individual catalytic reactions cannot be evaluated without the knowledge of the aluminum organization in the framework.

The search for new zeolites is of continuous interest in zeolite science. Significant effort is focused on the synthesis of new zeolites to meet the spatial and topologic requirements of individual catalytic reactions.[8] The TNU-9 zeolite (TUN[1] framework), which is a pentasil zeolite, is one of the most complex zeolites known, possessing 24 crystallographically distinguishable framework T sites equally populated in a monoclinic unit cell.[9] The projection of TUN along the *b* axis is very similar to that of MFI (ZSM-5 zeolite), but the connectivity in the third direction is more complex.[9a] The resulting 3D 10-ring channel system resembles that of MFI, but it has some unique features.[9a] The main difference between the two topologies is

[a] Dr. R. Karcz, Dr. J. Dedecek, Dr. B. Supronowicz, Dr. H. M. Thomas, P. Klein, Dr. E. Tabor, Dr. P. Sazama, Dr. V. Pashkova, Dr. S. Sklenak
J. Heyrovský Institute of Physical Chemistry, The Czech Academy of Sciences
Dolejskova 3, Prague 8, 182 23 (Czech Republic)
E-mail: stepan.sklenak@jh-inst.cas.cz

[b] Dr. R. Karcz
J. Haber Institute of Catalysis and Surface Chemistry
Polish Academy of Sciences, Niezapominajek 8, Cracow, 30-239 (Poland)

Supporting information and the ORCID identification number for the author of this article can be found under: https://doi.org/10.1002/chem.201605685.

the size of the channels (6.0×5.2 and 5.4×5.5 Å in TUN versus 5.1×5.5 and 5.3×5.6 Å in MFI) together with the presence of large cavities (7.2 Å) at crossings of the TUN channels.

TNU-9 has been investigated as a catalyst for both acid and redox reactions: Toluene[9b] and ethylbenzene[10] disproportionation, the methanol-to-hydrocarbons reaction (MTH),[11] the alkylation of benzene and toluene with methanol, ethanol, and isopropanol,[12] the isomerization and disproportionation of *m*-xyleme,[9b,13] the alkylation of benzene with *n*-hexane,[14] the hydroisomerization of *n*-hexane,[15] the alkylation of phenol with propylene,[16] and the disproportionation of *n*-propylbenzene[17] and isopropylbenzene[18] are examples of acid-catalyzed reactions that have been performed with the H-form of the TNU-9 zeolite. Redox-catalyzed reactions use transition-metal-exchanged TNU-9, for example, Co-TNU-9 and Cu-TNU-9, for the selective catalytic reduction of NO,[19] and Cu-TNU-9 for the oxidation of propane.[20] Studies have shown that the TNU-9 zeolite represents a highly promising zeolite matrix for both acid- and redox-catalyzed reactions. However, the potential of this new zeolite cannot be fully evaluated without the knowledge of the aluminum organization in the TUN framework, which is not currently known.

Because there are 24 crystallographically distinguishable framework T sites in the TUN framework, our ability to determine the aluminum siting is significantly limited, as shown in our prior studies of ZSM-5 zeolites that have the MFI[1] framework also with 24 T sites.[21] The TUN framework has the same size (10-ring) channels as the MFI framework. Therefore, the location of the framework aluminum atoms, and thus of the active sites compensating them, which can be either in the channels or at the channel intersections, is of great importance.[2,4] The location of aluminum in the channel system controls the void volume in which the active sites are located (less confined volume in the case of the channel intersections and more confined in the channels). The location of aluminum pairs (controlling the positions of divalent species) in the channel system is another key feature of silicon-rich zeolites.

Diffraction methods are of limited use in determining the structures of the cationic sites of divalent cations in the frameworks of silicon-rich zeolites. The structures of sites binding divalent cations have been estimated by using X-ray diffraction experiments only for the ferrierite[22] (Si/Al ratio 8.5) and mordenite[23] (Si/Al $\leq$8.5) frameworks and not for the MFI framework (ZSM-5 zeolite), which is a less complex analogue of the TUN framework.[9a] Furthermore, the TNU-9 zeolite has a low number of aluminum atoms in the framework (Si/Al 14) and a very large unit cell (five, four, and two times larger than the ferrierite, mordenite, and MFI frameworks, respectively). In addition, the structures of the cationic positions obtained from diffraction studies represent a superposition of different arrangements of these sites with and without accommodated divalent cations. Some rings corresponding to the cationic sites contain only one or no aluminum atom and are not able to accommodate a bare divalent cation. Therefore, to overcome the problems associated with diffraction methods, we have developed a new approach based on multiple spectroscopy and extensive periodic DFT computations that represents the only viable route for analyzing the siting of divalent cations in the TNU-9 zeolite at the present time.

In this article, we describe the use of ^{29}Si and ^{27}Al MAS NMR spectroscopy, Co^{II} as probes monitored by UV/Vis spectroscopy, and FTIR spectroscopy in tandem with periodic DFT calculations for investigating the aluminum distribution in the TUN framework and the location of aluminum pairs and divalent cations in extra-framework cationic positions of the TUN framework. The location of the α site in the TUN framework is proposed and six distinct 6-rings are suggested as plausible β sites.

Experimental Section

Sample preparation

TNU-9 with a Si/Al ratio of 14 was synthesized under hydrothermal conditions by using 1,4-dibromobutane (1,4-DBB, 99% Aldrich) and 1-methylpyrrolidine (1-MP 99% Aldrich) as organic structure-directing agents (OSDA) with a gel composition of 4.5 1,4-DBB, 13.5 1-MP, 11 Na_2O, 0.5 Al_2O_3, 30 SiO_2, and 1200 H_2O.[9b] The zeolite was synthesized by using gels prepared from NaOH (50% in water, Aldrich), $Al(NO_3)_3$ (Aldrich), fumed silica (Aerosil 200, Degussa), and deionized water. A small amount (2 wt% of the silica in the gel) of seed crystals were added to the mixture. After 1 h of vigorous stirring, the prepared gel was introduced into a stainless-steel reactor and heated at 433 K with agitation under autogenous pressure for 14 days. The obtained product was washed repeatedly with deionized water and dried at ambient temperature. The OSDA was removed by calcination of the sample at 823 K for 3 h under nitrogen and then for 20 h in a flow of air until the sample was white. The calcined sample was converted into the NH_4^+ and Na^+ forms by repeated (three times) equilibration of the zeolite with a 1.0 M solution (100 mL g^{-1}) of $NaNO_3$ and NH_4NO_3, respectively, for 24 h. Both the powder XRD patterns (Bruker D8 diffractometer, Bruker AXS, U.S.A) and SEM images (Jeol JSM-03 SEM microscope) evidenced a highly crystalline zeolite (see the Supporting Information).

Five samples, Co^{II},Na-TNU-9/a–e, with various degrees of Co^{II} exchange, with the Co/Al ratio ranging from 0.02 to 0.30 (Table 1), were prepared to characterize the aluminum distribution and the siting of divalent cations.

The Na-TNU-9 zeolite was equilibrated with aqueous solutions of $Co(NO_3)_2$ (Table 1) and then the samples were dried at ambient temperature. In addition, another sample, Ca,Na-TNU-9, was prepared for ^{27}Al MQ MAS NMR experiments. Na-TNU-9 was ion-exchanged three times with an aqueous solution of 0.1 M $Ca(NO_3)_2$ to obtain the Ca,Na-TNU-9 sample. The chemical compositions

Table 1. Chemical composition of the Co^{II},Na-TNU-9/a–e samples.

Sample	Si/Al	Co/Al	Co [mmol g^{-1}]	Bare Co^{II}[a] [mmol g^{-1}]
Co^{II},Na-TNU-9/a	14.2	0.02	0.02	0.01
Co^{II},Na-TNU-9/b	14.2	0.04	0.04	0.02
Co^{II},Na-TNU-9/c	14.2	0.13	0.13	0.11
Co^{II},Na-TNU-9/d	14.2	0.26	0.24	0.29
Co^{II},Na-TNU-9/e	14.2	0.30	0.28	0.29

[a] From FTIR analysis of [D_3]acetonitrile; [bare Co^{II}] = [Co Lewis sites].

(Table 1) of the cobalt-exchanged samples were determined by using XRF spectroscopy.

^{27}Al (3Q) and ^{29}Si MAS NMR spectroscopy

^{27}Al (3Q) and ^{29}Si MAS NMR spectra of the fully hydrated samples were measured on a Bruker Avance III HD 500 WB/US (11.7 T) spectrometer using ZrO_2 rotors with a rotation speed of 12 kHz for ^{27}Al MAS NMR and 7 kHz for ^{29}Si MAS NMR. The ^{29}Si MAS NMR single pulse spectrum, which is quantitative, of the Na-TNU-9 sample was collected by using a $\pi/2$ excitation pulse width of 4 μs and a relaxation delay of 30 s after 1536 scans. Cross-polarization (CP) pulse sequences with a 50% ramp CP pulse, 2000 μs contact time, a relaxation delay of 5 s, and 3072 scans were employed for collecting the ^{29}Si CP MAS NMR spectrum. The ^{29}Si isotropic chemical shifts were referenced to Q8M8. The ^{29}Si MAS NMR spectrum was simulated by using the dmfit software.[24]

The framework aluminum content (Si/Al_{FR}) was estimated by using[25] Equation (1):

$$Si/Al_{FR} = I/0.25I_1 \quad (1)$$

in which I denotes the total intensity of the ^{29}Si NMR signal in the single pulse experiment and I_1 denotes the intensity of the NMR line corresponding to the Si(3Si,1Al) atoms.

The Ca,Na form of TNU-9 was used for ^{27}Al (3Q) MAS NMR experiments to prevent the effect of a high local density of solvated monovalent cations on the local geometry of AlO_4^- in Al-O-(Si-O)$_2$-Al. Ca^{2+} cations compensate for two aluminum atoms in Al-O-(Si-O)$_2$-Al sequences, whereas Na^+ cations compensate for a single isolated aluminum.[26] The ^{27}Al MAS NMR spectrum, which is quantitative, was acquired by using a high-power decoupling pulse sequence with an excitation $\pi/6$ pulse width of 2 μs and a relaxation delay of 2 s. The ^{27}Al 3Q MAS NMR experiment was performed by using the *z*-filtered three-pulse sequence with excitation, conversion, and selective pulse widths of 4.6, 1.6, and 20 μs, respectively, and a relaxation delay of 0.5 s. The ^{27}Al isotropic chemical shifts were referenced to the aqueous solution of $Al(NO_3)_3$. Both the ^{27}Al MAS NMR and the ^{27}Al 3Q MAS NMR spectra were simultaneously fitted with the dmfit software[24] by using the "Czjzek simple" model to obtain the ^{27}Al NMR parameters. The ^{27}Al 3Q MAS NMR spectroscopic analysis of silicon-rich zeolites has been discussed by van Bokhoven et al.[27] and Sarv et al.,[28] and the 3Q MAS NMR technique is explained in detail by Alemany.[29]

UV/Vis spectroscopy of the Co^{II}-exchanged TNU-9 samples

The siting as well as the distribution of bare Co^{II} in cationic sites in the dehydrated Co^{II},Na-TNU-9 samples were investigated by employing UV/Vis spectroscopy. The UV/Vis reflectance spectra of dehydrated samples were recorded on a PerkinElmer Lambda 950 UV/Vis-NIR spectrometer equipped with an integrating sphere for diffuse-reflectance measurements covered by Spectralon®. Spectralon® also served as a reference. Dehydrated samples were prepared by heating grained (0.3–0.5 mm) Co-TNU-9 samples at 770 K under a dynamic vacuum of 8×10^{-2} Pa in a silica flask connected to a silica optical cell. Dehydration was carried out in two steps, at 370 K for 30 min and at 770 K for 3 h, with a heating ramp of 5 K min^{-1}. After dehydration, the sample was cooled to ambient temperature and transferred under vacuum to the 5 mm optical cell and sealed. The reflectance was recalculated by using the Schuster–Kubelka–Munk function $F(R_\infty)=(1-R_\infty)2/2R_\infty$, in which R_∞ is the diffuse reflectance from a semi-infinite layer and $F(R_\infty)$ is proportional to the absorption coefficient. After the baseline abstraction, the spectra of the samples in the region of the Co^{II} d–d transitions were simulated by using Gaussian bands employing the Origin 8.1 software (OriginLab, Northampton, MA).

Since Origin and OriginPro are well established commercial software products, you will only need to cite OriginLab in the Materials and Method section of your publication. The simplest form is to reference the Origin software without version, like this: Origin (OriginLab, Northampton, MA).

FTIR spectroscopy

FTIR spectra were recorded at 298 K on a Nicolet 6700 spectrometer operating at a resolution of 2 cm^{-1} by collecting 128 scans for a single spectrum. The samples were analyzed as self-supported pellets with a thickness of 10 mg cm^{-2}. The samples were evacuated at 723 K for 3 h and subsequently the FTIR spectra were recorded to monitor antisymmetric T-O-T stretching lattice vibrations. Following that, [D_3]acetonitrile (1.3 kPa) was adsorbed on the samples for 15 min at 298 K and subsequently the samples were evacuated for 15 min at 473 K. Then, FTIR spectra of the adsorbed [D_3]acetonitrile were recorded. The spectra intensities were normalized by using the integral area of the zeolite skeletal bands in the region between 1750 and 2100 cm^{-1}. The positions and relative intensities of the bands of the antisymmetric T-O-T stretching lattice vibrations and of the adsorbed [D_3]acetonitrile were analyzed by using the Origin 7.5 software assuming Gaussian profiles.[30]

Analysis of the aluminum distribution

The distribution of aluminum atoms in the zeolite is described by Equations (2)–(4):

$$[Al_{total}] = [Al_{single}] + [Al_{pair}] \quad (2a)$$

or

$$[Al_{total}] = [Al_{single}] + [Co_\alpha] + [Co_\beta] + [Co_\gamma] \quad (2b)$$

$$[Al_{single}] = [Al_{total}] - 2[Co_{max}] \quad (3a)$$

or

$$[Al_{single}] = [Al_{total}] - 2([Co_\alpha] + [Co_\beta] + [Co_\gamma]) \quad (3b)$$

$$[Al_{pair}] = 2[Co_{Lewis}] \quad (4a)$$

or

$$[Al_{pair}] = 2([Co_\alpha] + [Co_\beta] + [Co_\gamma]) \quad (4b)$$

in which $[Al_{total}]$ represents the concentration of all the aluminum atoms present in the sample, $[Al_{single}]$ and $[Al_{pairs}]$ correspond to the concentrations of the isolated single aluminum atoms and aluminum in the Al-O-(Si-O)$_2$-Al sequences, respectively, $[Co_\alpha]$, $[Co_\beta]$, and $[Co_\gamma]$ are the concentrations of Co^{II} at the α, β, and γ sites, respectively, obtained from the FTIR spectra of shifted antisymmetric T-O-T stretching lattice vibrations, $[Co_{max}]$ corresponds to the $[Co^{II}(H_2O)_6]^{2+}$ ion exchange capacity, and $[Co_{LEWIS}]$ corresponds to the concentration of Co^{II} Lewis sites observed in the FTIR spectra of adsorbed [D_3]acetonitrile. Details regarding the analysis of the aluminum distribution are discussed elsewhere.[2]

Possible cationic sites in TNU-9

Three types of cationic sites for bare divalent metal cations, designated as α, β, and γ, have been reported for pentasil zeolites.[2, 5, 30d] The cationic sites are formed by Al-O-(Si-O)$_2$-Al sequences located in 6-ring or more complex structures. The presence of two aluminum atoms in the site is necessary for the stabilization of bare divalent cations.[3a, 6a, b, 31] Al-O-Si-O-Al sequences are not present in silicon-rich materials.[32] Visual inspection of the TUN framework revealed analogous structures for this zeolite as well. Based on this analogy and analysis of the spectroscopic results (see the Discussion), the rings investigated by periodic DFT calculations as possible cationic sites were proposed. The γ site was not calculated by periodic DFT because the concentration of framework aluminum atoms forming the γ site in the TNU-9 sample was very low (see the Experimental Section). The locations of the α cationic site and possible β cationic sites in the TUN framework are depicted in Figure 1.

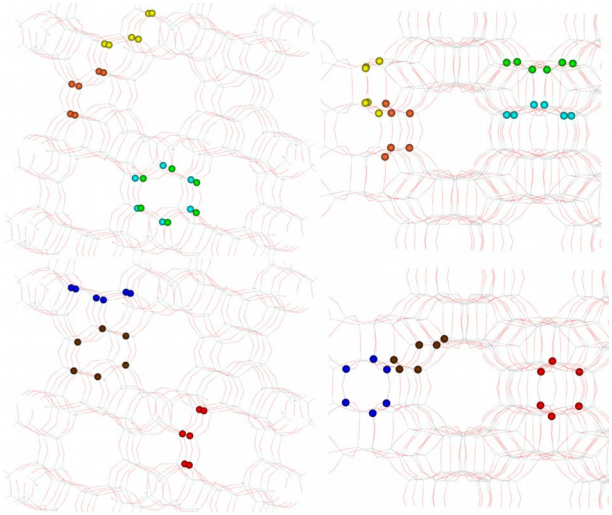

Figure 1. Locations of the α cationic site (● top), the $\beta_{T5T2T22}$ (● top), β_{T9T6T4} (● top), $\beta_{T11T4T9}$ (● bottom), $\beta_{T8T10T11}$ (● bottom), $\beta_{T14T12T21}$ (● top), and $\beta_{T23T19T17}$ (● bottom) sites in the TUN framework. Views along the straight (left) and sinusoidal (right) channels.

α cationic site: This site represents an elongated 6-ring (T22-T18-T24-T10-T11-T4) composed of two 5-rings (Figure 2). There are two possible aluminum sitings in the 6-rings: The two aluminum atoms occupy either T4 and T24 or T10 and T22. The α sites of mordenite, ferrierite, ZSM-5, and TNU-9 are very similar.

Possible β cationic sites: The β sites in ferrierite, ZSM-5, and the β-zeolite correspond to various deformed 6-rings. Thus, based on the TUN topology, we suggest six distinct 6-rings as plausible β sites in the TUN framework.

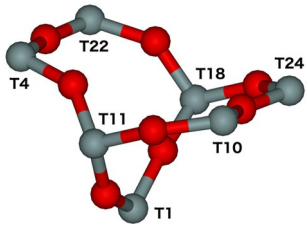

Figure 2. Structure of the α cationic site. T atoms (Si or Al) are in gray and oxygen atoms in red.

$\beta_{T5T2T22}$ and β_{T9T6T4} sites: The deformed 6-rings formed by the T5-T2-T22-T5-T2-T22 and T9-T6-T4-T9-T6-T4 atoms create the $\beta_{T5T2T22}$ and β_{T9T6T4} sites, respectively (Figure 3). The two aluminum atoms

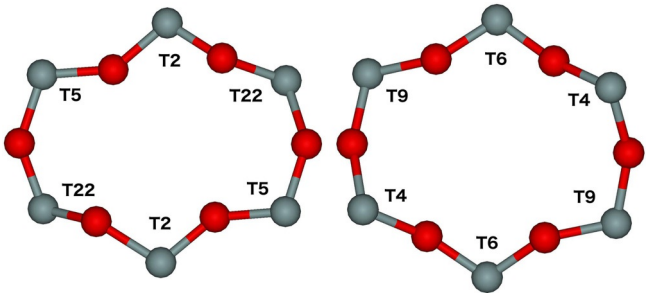

Figure 3. Structures of the $\beta_{T5T2T22}$ (left) and β_{T9T6T4} (right) cationic sites. T atoms (Si or Al) are in gray and oxygen atoms in red.

can occupy either T5 and T5 or T2 and T2 or T22 and T22 in the former ring and either T9 and T9 or T6 and T6 or T4 and T4 in the latter ring (Figure 3).

$\beta_{T11T4T9}$ and $\beta_{T8T10T11}$ sites: The two sites are formed by elongated 6-rings (T11-T4-T9-T9-T4-T11 and T8-T10-T11-T11-T10-T8; Figure 4). The two aluminum atoms can be accommodated in either T11 and T9 or T4 and T4 in the former ring and either T11 and T8 or T10 and T10 in the latter ring.

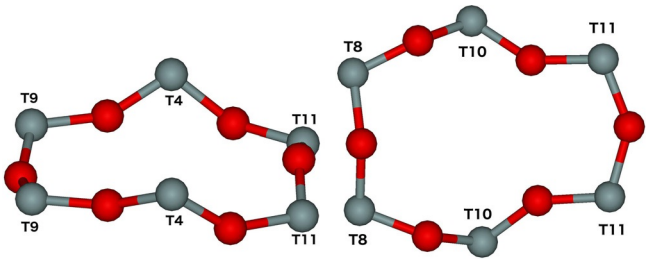

Figure 4. Structures of the $\beta_{T11T4T9}$ (left) and $\beta_{T8T10T11}$ (right) cationic sites. T atoms (Si or Al) are in gray and oxygen atoms in red.

$\beta_{T14T12T21}$ site: Two aluminum atoms located in either the T14 and T21 or T12 and T12 positions of the 6-ring composed of the T14-T12-T21-T21-T12-T14 atoms yield the $\beta_{T14T12T21}$ site (Figure 5).

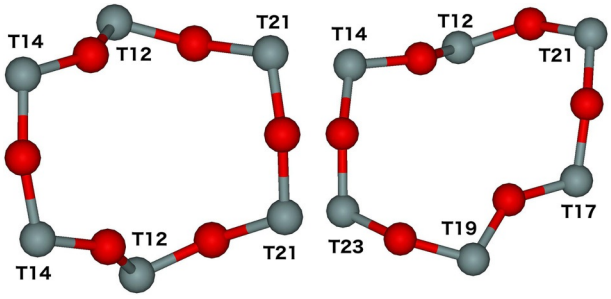

Figure 5. Structures of the $\beta_{T14T12T21}$ (left) and $\beta_{T23T19T17}$ (right) cationic sites. T atoms (Si or Al) are in gray and oxygen atoms in red.

$\beta_{T23T19T17}$ site: The 6-ring comprised of the T23-T19-T17-T21-T12-T14 atoms creates the $\beta_{T23T19T17}$ site (Figure 5). There are three possible aluminum sitings in the 6-ring: The two aluminum atoms are positioned in either T23 and T21 or T19 and T12 or T17 and T14 sites.

Computational models and methods

Computational models: Seventeen models (Table 2) possessing *P*1 symmetry were employed. They feature one unit cell of TUN with two Al/Si substitutions forming the cationic sites accommodating a Co^{II}. The starting monoclinic structure was downloaded from the zeolite structural database.[1]

Table 2. Computational models employed in the computational study.

Model	Cationic site	Al sitings in the 6-rings	Optimization
α(T4T24)	α	T4 and T24	yes
α(T10T22)	α	T10 and T22	yes
$\beta_{T5T2T22}$(T5T5)	$\beta_{T5T2T22}$	T5 and T5	no
$\beta_{T5T2T22}$(T2T2)	$\beta_{T5T2T22}$	T2 and T2	no
$\beta_{T5T2T22}$(T22T22)	$\beta_{T5T2T22}$	T22 and T22	no
β_{T9T6T4}(T9T9)	β_{T9T6T4}	T9 and T9	no
β_{T9T6T4}(T6T6)	β_{T9T6T4}	T6 and T6	no
β_{T9T6T4}(T4T4)	β_{T9T6T4}	T4 and T4	no
$\beta_{T11T4T9}$(T11T9)	$\beta_{T11T4T9}$	T11 and T9	yes
$\beta_{T11T4T9}$(T4T4)	$\beta_{T11T4T9}$	T4 and T4	no
$\beta_{T8T10T11}$(T11T8)	$\beta_{T8T10T11}$	T11 and T8	yes
$\beta_{T8T10T11}$(T10T10)	$\beta_{T8T10T11}$	T10 and T10	no
$\beta_{T14T12T21}$(T14T21)	$\beta_{T14T12T21}$	T14 and T21	yes
$\beta_{T14T12T21}$(T12T12)	$\beta_{T14T12T21}$	T12 and T12	no
$\beta_{T23T19T17}$(T23T21)	$\beta_{T23T19T17}$	T23 and T21	yes
$\beta_{T23T19T17}$(T19T12)	$\beta_{T23T19T17}$	T19 and T12	yes
$\beta_{T23T19T17}$(T17T14)	$\beta_{T23T19T17}$	T17 and T14	yes

Electronic structure calculations: Periodic DFT calculations were carried out by employing the VASP code.[33] The high-spin electron configuration cobalt $d^{5\uparrow}d^{2\downarrow}$ was employed for the Co^{II} accommodated in the zeolite. The Kohn–Sham equations were solved variationally in a plane-wave basis set using the projector-augmented wave (PAW) method of Blöchl,[34] as adapted by Kresse and Joubert.[35] The exchange-correlation energy was described by the PW91 generalized gradient approximation (GGA) functional.[36] Brillouin zone sampling was restricted to the Γ point. A plane-wave cutoff of 400 eV was utilized for geometry optimizations and a smaller cutoff of 300 eV was used for the molecular dynamics simulations.

Geometry optimizations: Only eight models (Table 2), selected on the basis of our ^{27}Al 3Q MAS NMR experiments, were optimized (see the Discussion). The atomic positions were optimized at constant volume by employing a conjugate-gradient algorithm minimization of energies and forces whereas the lattice parameters were fixed at their experimental values.

Molecular dynamics: The molecular dynamics (MD) simulations were carried out on all the 17 models. The MD computations used the exact Hellmann–Feynman forces acting on atoms and applied the statistics of canonical ensemble to the motion of the atomic nuclei[37] by using the Verlet velocity algorithm[38] to integrate Newton's equations of motion. The time step for the integration of the equations of motion was 1 fs. The simulations were run for 4000 fs at 400 K. Visual inspection of the structures along the MD trajectories showed that the duration of the MD simulations was long enough, because it included both the rearrangements of the local structures of the TUN framework for some cationic sites (up to ca. 1000 fs) as well as a long period (ca. 3000 fs) when the system fluctuated around the equilibrium and "snapshots" were collected and optimized. Similar time lengths were used for MD simulations of cationic sites in ferrierite.[3a,31,39] The structures of eight distinct "snapshots" collected at 500, 1000, 1500, … 4000 fs of the molecular dynamics simulations were optimized for the eight selected models (Table 2).

Results

^{29}Si MAS NMR spectroscopy

The ^{29}Si MAS NMR spectrum of the TNU-9 sample (Figure 6) is similar to that already reported in the literature.[9b] Our simulation of the spectrum revealed six ^{29}Si NMR resonances at −117, −115, −110, −107, −104, and −98 ppm. Because ^{29}Si NMR resonances with chemical shifts between −92 and −100 ppm reflect Si(3Si,1OH) atoms,[40] the measured ^{29}Si NMR resonance at −98 ppm was attributed to Si(3Si,1OH) atoms. This was further confirmed by its significant increase in the cross-polarization experiment (not shown in the figures). Because ^{29}Si NMR resonances between −97 and −107 ppm correspond to Si(3Si,1Al) atoms,[40] and those between −108 and −115 are characteristic of signals of Si(4Si,0Al) atoms,[40] the observed ^{29}Si NMR resonances at −117, −115, and −110 ppm and those at −107 and −104 ppm were assigned to Si(4Si,0Al) and Si(3Si,1Al) atoms, respectively. The Si/Al ratio of 14.2 obtained from the chemical analysis using the X-ray fluorescence (XRF) method is in good agreement with the Si/Al_{FR} ratio of 13.8 determined from the ^{29}Si MAS NMR spectrum by employing Equation (1). This agreement confirms the assignment of the ^{29}Si NMR resonances and moreover reveals that Si(2Si,2Al), Si(1Si,3Al), and extra-framework aluminum atoms are not present in the investigated zeolite.

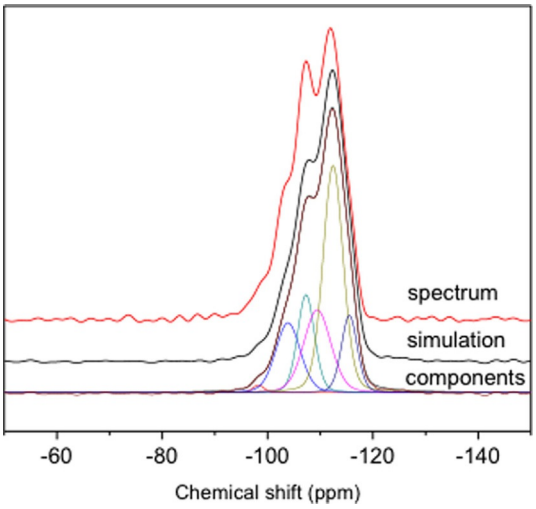

Figure 6. ^{29}Si MAS NMR spectrum of the Na-TNU-9 sample along with the simulated spectrum with Gaussian bands of individual resonances.

^{27}Al (3Q) MAS NMR spectroscopy

The ^{27}Al MAS NMR single pulse spectrum of the hydrated zeolite is shown in Figure 7. Only one ^{27}Al NMR resonance centered at 55 ppm is observed, which reflects the exclusive presence of tetrahedral framework aluminum atoms. ^{27}Al NMR resonances at around 0 ppm as well as between 15 and 30 ppm corresponding to extra-framework octahedral and penta-coordinated aluminum atoms, respectively, are not observed.

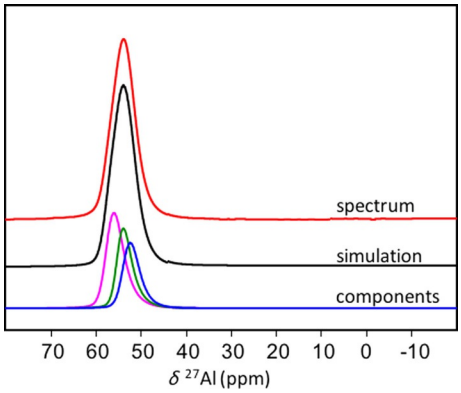

Figure 7. ^{27}Al MAS NMR spectrum of the Ca,Na-TNU-9 sample along with the simulated spectrum with individual ^{27}Al NMR resonances.

On-sight analysis of the ^{27}Al 3Q MAS NMR spectrum depicted in Figure 8 indicates the presence of at least two ^{27}Al NMR resonances in the spectrum of Ca,Na-TNU-9.

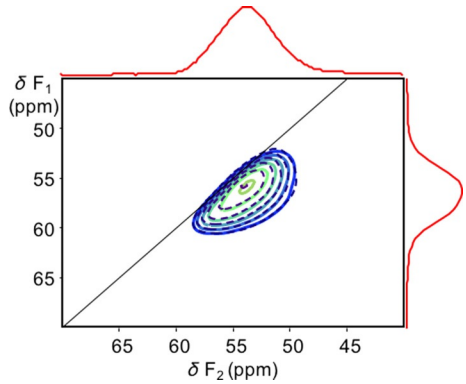

Figure 8. 2D plot of the ^{27}Al 3Q MAS NMR spectrum of the Ca,Na-TNU-9 sample (black), F_1 and F_2 projections (red), and simulated spectrum (blue and green).

Detailed analysis employing a simulation of the 2D spectrum confirmed the presence of three ^{27}Al NMR resonances with isotropic chemical shifts at 53.5, 55.0, and 57.2 ppm. Table 3 presents the isotropic chemical shifts (σ_i), the corresponding nuclear quadrupolar coupling products (P_Q), and the concentrations of aluminum atoms corresponding to the ^{27}Al NMR resonances for the TNU-9 zeolite.

Values of the nuclear quadrupolar coupling product (P_Q) lower than 2.5 MHz correspond to typical tetrahedral aluminum atoms in the zeolite framework.[3c] P_Q values <2.5 MHz indicate negligible quadrupolar broadening of the ^{27}Al NMR resonances of aluminum occupying framework T sites and confirm the reliability of the spectral simulation. Because the presence of a second aluminum atom in a Al-O-(Si-O)$_2$-Al sequence can significantly change the corresponding isotropic chemical shift of the aluminum atom,[26,41] the presence of three ^{27}Al NMR resonances reveals the location of aluminum atoms in at least (aluminum atoms accommodated in several framework T sites can exhibit indistinguishable ^{27}Al isotropic chemical shifts) two framework T sites (schematically, e.g., single Al(T_X) and Al(T_Y) atoms and aluminum atoms in Al(T_X)-O-(Si-O)$_2$-Al(T_X) sequences). The concentrations of aluminum atoms located in different framework T sites are 30 and 40% (Table 3).

Table 3. Isotropic chemical shifts (σ_i) and the nuclear quadrupolar coupling products (P_Q) of the ^{27}Al NMR resonances of framework aluminum atoms and the relative concentrations of aluminum atoms corresponding to the individual resonances.

$\sigma_i^{[a]}$ [ppm]	$P_Q^{[a]}$ [MHz]	$\sigma_i^{[b]}$ [ppm]	$P_Q^{[b]}$ [MHz]	Al$^{[b]}$ [%]
57.2	2.2	57.2	2.3	40
55.0	2.2	55.0	2.2	30
53.5	2.1	53.5	2.1	30

[a] From ^{27}Al 3Q MAS NMR experiments. [b] From ^{27}Al MAS NMR measurements.

FTIR spectroscopy

Figure 9A shows the FTIR spectra of [D_3]acetonitrile adsorbed on the samples Co,Na-TNU-9/a–e. Five bands can be identified in the spectra: 1) A very low-intensity band at 2330 cm^{-1} corresponding to framework aluminum Lewis acid sites, 2) a band at 2305 cm^{-1} reflecting Co^{II} Lewis acid sites of bare Co^{II}, 3) a band at 2280 cm^{-1} corresponding to Na$^+$ cations, 4) a band at

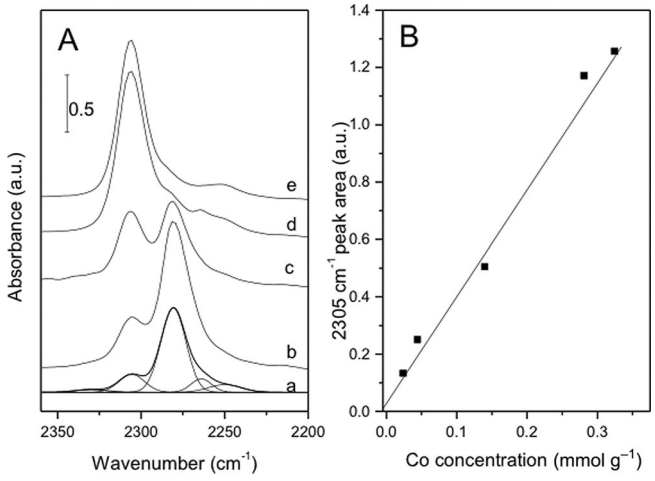

Figure 9. A) FTIR spectra of [D_3]acetonitrile adsorbed on the Co,Na-TNU-9/a–e samples together with the simulated spectrum of Co,Na-TNU-9/a and B) the effect of cobalt loading on the integrated intensity of the peak of [D_3]acetonitrile adsorbed on cobalt Lewis sites.

2264 cm^{-1} related to terminal silanol groups (SiOH), and 5) a band at 2248 cm^{-1} for [D_3]acetonitrile physisorbed on the surface.[42] The extinction coefficient of [D_3]acetonitrile adsorbed on Co^{II}, which is $\varepsilon = 11(\pm 0.5)$ cm mmol g^{-1}, was determined based on the premise that the intensity of the band of [D_3]acetonitrile at 2305 cm^{-1} increases linearly with the cobalt loading in the whole cobalt concentration range (Figure 9B). The concentrations of bare Co^{II} corresponding to Co^{II} Lewis acid sites in the individual Co,Na-TNU-9/a–e samples are listed in Table 1.

Figure 10 shows the FTIR spectra of the dehydrated Co,Na-TNU-9/a–e samples in the region of the T-O-T vibrations of the zeolite framework (960–880 cm^{-1}). The broad band in the

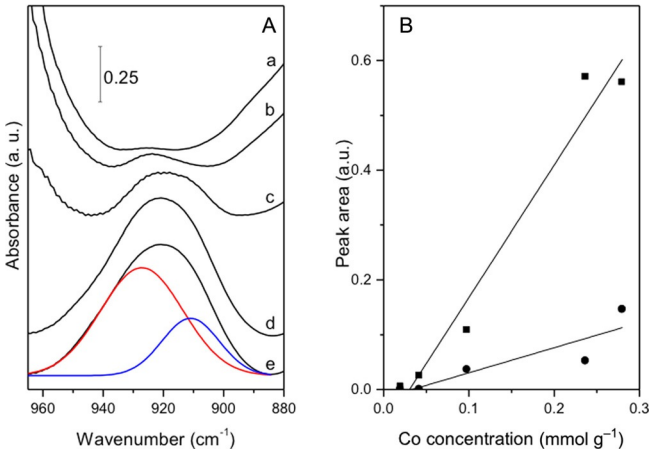

Figure 10. A) FTIR spectra of the Co,Na-TNU-9/a–e samples dehydrated at 723 K in the 960–880 cm^{-1} region together with the simulated spectrum of Co,Na-TNU-9/e to the Gaussian bands of Co^{II} in the individual sites. B) The effect of the cobalt loading on the integrated area of bands at 930 (■) and 910 cm^{-1} (●).

range 960–880 cm^{-1} confirms the presence of bare Co^{II} in the TUN framework. The band reflects the perturbation of the T-O-T vibrations due to the coordination of bare Co^{II} to the framework oxygen atoms of the ring forming the cationic sites in dehydrated zeolites.[30] Analysis of the spectra reveals two maxima at 930 and 910 cm^{-1}, which evidences the location of Co^{II} in two cationic sites. The intensities of the two bands concurrently increase with increasing cobalt loading revealing no preferential formation of one of the cationic sites. The synchronous increase in the intensities of the two bands rules out the possibility of estimating the extinction coefficients of the individual Co^{II} species of the two bands.

UV/Vis spectroscopy

The UV/Vis spectra of the dehydrated Co,Na-TNU-9/a–e samples with different cobalt loadings are shown in Figure 11. The absorption in the visible region between 12500 and 25000 cm^{-1} corresponds to the d–d transitions of bare Co^{II} accommodated in the cationic sites of the dehydrated zeolites. The bands in the UV region above 38000 cm^{-1} can be assigned to charge transfer, typically $O \rightarrow Co^{II}$.[2,6a] None of the spectra show bands

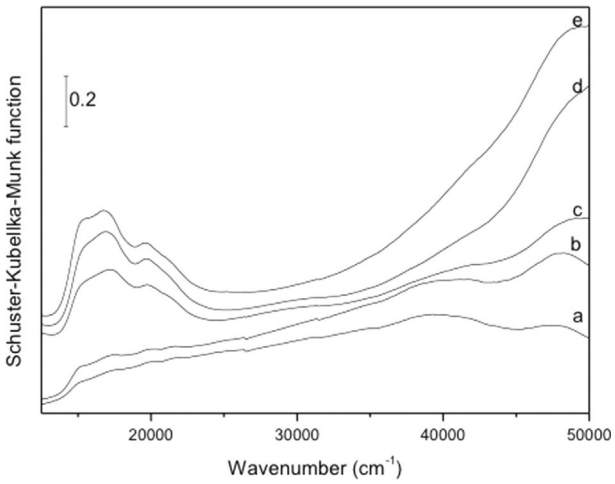

Figure 11. UV/Vis spectra of the Co^{II},Na-TNU-9/a–e samples dehydrated at 723 K.

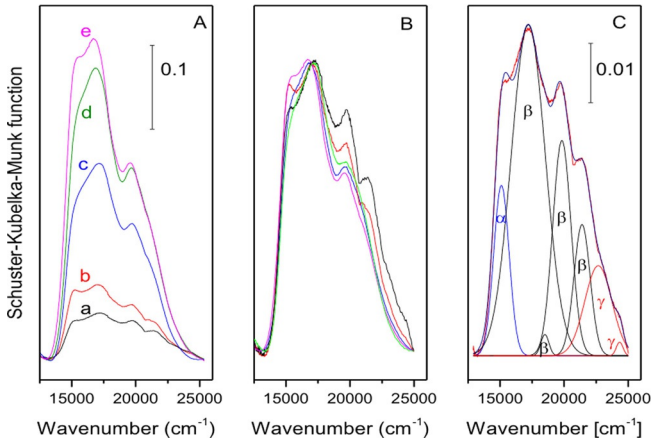

Figure 12. A) Visible, and B) normalized visible spectra of the Co^{II},Na-TNU-9/a–e samples, and C) a simulation of the visible spectrum of Co^{II},Na-TNU-9/b showing bands corresponding to Co^{II} in the α, β, and γ cationic sites.

at around 33000 cm^{-1} reflecting the formation of Co–oxo bridging species.[30d] Figure 12 shows the visible spectra of Co^{II} in the dehydrated samples.

A detailed inspection of the normalized spectra with various cobalt loadings reveals the presence of three spectroscopic species. The first corresponds to the absorption at around 15000 cm^{-1}, the second appears in the central part of the spectra, and the third, observable only at low cobalt loadings, has absorptions above 20000 cm^{-1}. The spectral simulations and analyses of their second derivatives evidenced seven bands in each spectrum. The effect of cobalt loading on the intensities of individual bands allowed their assignment to three spectroscopic species corresponding to Co^{II} accommodated in the α, β, and γ sites. Based on the results of our prior studies,[3b,5,30d] we can deduce that the band at 15050 cm^{-1}, the quartet at 16700, 18000, 19300, and 20900 cm^{-1}, and the doublet at 22400 and 23000 cm^{-1} correspond to Co^{II} located in the α, β, and γ sites, respectively (Table 4).

Table 4. Wavenumbers and extinction coefficients of bare Co^{II} accommodated in the α, β, and γ sites in the ZSM-5, ferrierite, mordenite, and TNU-9 zeolites.

Zeolite	ν_α [cm^{-1}]	k_α [10^{-3} g mol^{-1} cm^{-1}]	ν_β [cm^{-1}]				k_β [10^{-3} g mol^{-1} cm^{-1}]	ν_γ [cm^{-1}]		k_γ [10^{-3} g mol^{-1} cm^{-1}]
ZSM-5	15100	3.7±1.1	16000	17150	18600	21200	2.7±0.7	20100	22000	0.9±0.6
ferrierite	15000	2.7±1.1	16000	17100	18700	20600	2.5±0.7	20300	22000	1.1±0.5
mordenite	14800	7.3±3.1	15900	17500	19200	21000	2.7±0.7	20150	22050	1.9±1.0
TNU-9	15050	–	16700	18000	19300	20900	–	22400	23000	–

The area of the doublet assigned to the γ site is only 0.1% of the total Co^{II} peak area for the sample with maximum Co^{II} loading, and, moreover, the doublet is only well developed in the spectra with the lowest cobalt loading. Therefore, these two bands have been omitted from further analysis.

The intensities of the bands corresponding to Co^{II} located in the α and β sites concurrently increase with increasing cobalt loading and reveal no preferential formation for one of the cationic sites at low as well as at high cobalt loading. Thus, the extinction coefficients corresponding to Co^{II} accommodated in the α and β sites cannot be calculated because there is no set of at least two independent equations describing the dependence of the spectral intensities on the cobalt loading. Therefore, only the average extinction coefficient of the Co^{II} absorption in the range between 14000 and 25000 cm^{-1} can be estimated ($k=(6\pm1)\times10^{-5}$ g mol^{-1} cm^{-1}).

Computational Results

Structures and stability of the α and possible β cationic sites

Our MD calculations of the 17 computational models (Table 2) revealed that the 6-ring forming the α cationic site as well as the six 6-rings creating six possible β cationic sites with all the possible aluminum sitings in the 6-rings (Table 2) could accommodate bare Co^{II}. The MD results showed the proper binding of Co^{II} mainly to the oxygen atoms of the AlO_4^- tetrahedra and significant rearrangements of the local structures of the zeolite framework at some cationic sites.

The subsequent optimizations of the two models of the α site and the six selected models of the β sites (see the Discussion section) yielded the structures of Co^{II} exchanged in the corresponding cationic sites, the relative binding energies[3a] of Co^{II} in these sites, and the stabilization energies[3a,31] of the cationic sites accommodating Co^{II} (Table 5).

Our MD simulations of the α(T10T22) and α(T4T24) models of the α site as well as the $\beta_{T11T4T9}$(T11T9) and $\beta_{T14T12T21}$(T14T21) models of the β sites and subsequent optimizations of selected MD snapshots led to energy stabilizations by 5, 5, 11, and 2 kcal mol^{-1}, respectively (Table 5), relative to the same models that were not relaxed employing MD simulations but simply optimized by using the structure downloaded from the zeolite structural database.[1] These four sites noticeably rearranged during the MD computations. Conversely, there is no rearrangement observed for the $\beta_{T8T10T11}$(T11T8), $\beta_{T23T19T17}$(T23T21), $\beta_{T23T19T17}$(T19T12), and $\beta_{T23T19T17}$(T17T14) sites (Table 5). Similarly, the β cationic sites of the β-zeolite do not rearrange either.[3b]

Table 5. Relative binding energies[3a] of Co^{II}, stabilization energies,[3a,31] the number of oxygen atoms in the AlO_4^- and SiO_4 tetrahedra to which Co^{II} is bound, and affirmation of near-planarity.

Model	ΔBE_{Co}[a] [kcal mol^{-1}]	ΔE_{stab}[b] [kcal mol^{-1}]	O[Al]	O[Si]	Near-planarity
α(T10T22)	15.6	5.3	4	1	yes
α(T4T24)	12.1	5.3	4	1	yes
$\beta_{T11T4T9}$(T11T9)	13.4	10.5	4	0	yes
$\beta_{T8T10T11}$(T11T8)	17.5	0.0	3	1	yes
$\beta_{T14T12T21}$(T14T21)	15.4	2.0	4	0	no
$\beta_{T23T19T17}$(T23T21)	19.4	0.0	2	2	no
$\beta_{T23T19T17}$(T19T12)	4.5	0.0	3	1	no
$\beta_{T23T19T17}$(T17T14)	0.0	0.0	4	0	yes

[a] The difference between the energies of the Co-TNU-9 featuring the site of interest and the Co-TNU-9 with the most stable site (i.e., $\beta_{T23T19T17}$(T17T14)). This energy gap is corrected by subtracting the difference between the energies of the TNU-9 with the empty site of interest and the TNU-9 featuring the most stable site without the cation. The empty sites have two aluminum atoms in the corresponding six-membered ring forming the cationic sites that are not compensated by any cation. [b] The difference between the energies of the model relaxed by MD simulations and subsequently optimized and the model that was not relaxed by MD simulations but simply optimized using the starting structure downloaded from the zeolite structural database (see ref. [1]).

The computational results (Table 5) also revealed the relative binding energies of Co^{II} in the calculated cationic sites. The cation binds the most tightly in the $\beta_{T23T19T17}$(T17T14) site, followed by in the $\beta_{T23T19T17}$(T19T12) site. The binding is the weakest in the $\beta_{T23T19T17}$(T23T21) site.

The optimized structures of the eight models (Table 5) are shown in Figures 13–16. Whether the optimized structures are near-planar or not is indicated in Table 5.

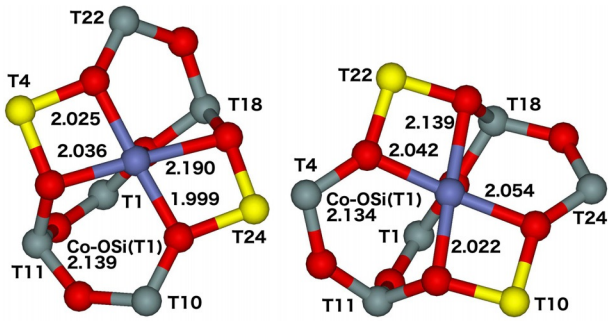

Figure 13. Optimized structures of the α(T4T24) (left) and α(T10T22) (right) models. The distances are in Å. Silicon atoms are in gray, oxygen atoms in red, aluminum atoms in yellow, and the cobalt atom in blue.

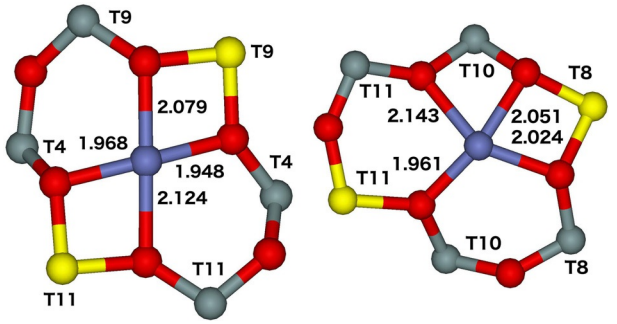

Figure 14. Optimized structures of the $\beta_{T11T4T9}$(T11T9) (left) and $\beta_{T8T10T11}$(T11T8) (right) models. The distances are in Å. Silicon atoms are in gray, oxygen atoms in red, aluminum atoms in yellow, and the cobalt atom in blue.

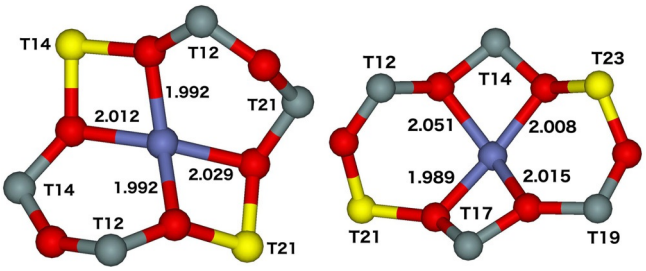

Figure 15. Optimized structures of the $\beta_{T14T12T21}$(T14T21) (left) and $\beta_{T23T19T17}$(T23T21) (right) models. The distances are in Å. Silicon atoms are in gray, oxygen atoms in red, aluminum atoms in yellow, and the cobalt atom in blue.

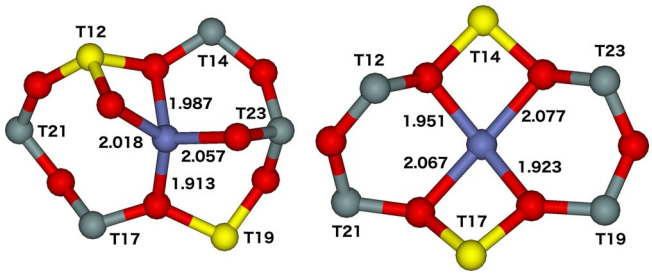

Figure 16. Optimized structures of the $\beta_{T23T19T17}$(T19T12) (left) and $\beta_{T23T19T17}$(T17T14) (right) models. The distances are in Å. Silicon atoms are in gray, oxygen atoms in red, aluminum atoms in yellow, and the cobalt atom in blue.

The Co–O_{Al} and Co–O_{Si} bond lengths (Figures 13–16) range from 1.913 to 2.190 Å and from 2.015 to 2.143 Å, respectively. The calculated Co–O bond lengths are in good agreement with those obtained by EXAFS measurements, which revealed two Co–O distances of 1.99 and 2.09 Å for Co-ferrierite with Co^{II} located mainly in the β sites.[43]

Discussion

Aluminum distribution in the framework

The ^{27}Al (3Q) MAS NMR spectra of the Ca,Na-TNU-9 sample (Figures 7 and 8) show the presence of framework tetrahedral aluminum atoms and the absence of any extra-framework aluminum species. The ^{29}Si MAS NMR experiments clearly revealed the absence of Si(2Si,2Al) and Si(1Si,3Al) atoms, thereby excluding the existence of Al-O-Si-O-Al sequences in the framework of the TNU-9 sample. Therefore, the two aluminum atoms of the aluminum pairs in the 6-rings forming cationic sites for divalent cations are separated by two silicon atoms (i.e., they create Al-O-(Si-O)$_2$-Al sequences).

Table 1 shows that the maximum ion-exchange capacity of the zeolite for the divalent Co^{II} hexaaqua complex is 60% (Co/Al 0.3). The isolated single aluminum atoms thus represent 40% of all the aluminum atoms [Equations (3a) and (3b)]. The concentration of bare Co^{II} in extra-framework positions reflected as acid Lewis sites that interact with [D_3]acetonitrile in the dehydrated zeolite loaded with maximum Co^{II} is 0.29 mmol g^{-1} (Table 1). This value agrees well with the cobalt concentration in the zeolite, which is 0.28 mmol g^{-1} (Table 1). This agreement indicates that all the cobalt species in the dehydrated zeolite are present as bare Co^{II} balancing two aluminum atoms located in one ring. It should be noted that Me^{II} (Me^{II} = divalent metal cation) accommodated in the vicinity of two aluminum framework atoms located in two different rings exhibit very high energies.[44] Therefore, the formation of some Co–oxo species is expected for Co^{II} in the proximity of such organized aluminum atoms in two different rings. Various charged bridging Co–oxo species were suggested to exist in some Co-zeolites.[2] The exact nature of these Co–oxo species is not clear but they have to be balanced by aluminum atoms unable to accommodate bare Co^{II}. These aluminum atoms either form Al-O-(Si-O)$_{n>2}$-Al sequences in large rings (more than 6-rings) or are located in two different rings. These Co–oxo bridging species are reflected in the absorption band in the UV region at around 33 000 cm^{-1}.[30d] The UV/Vis spectra of the dehydrated Co^{II},Na-TNU-9/a–e samples (Figure 11) show the absence of any band at around 33 000 cm^{-1} and thus reveal that Co–oxo bridging species are not formed. Besides the above-mentioned bridging Co–oxo species, UV/Vis and FTIR "invisible" Co–oxo species (not adsorbing [D_3]acetonitrile) have been reported to represent a significant fraction of Co^{II} in some samples of the β-zeolite.[45] Recently, these Co–oxo species were attributed to $[Co^{III}O]^+$ cations balancing one aluminum atom.[46] Because exclusively hexaaqua complexes of Co^{II} are exchanged in the zeolite, these $[Co^{III}O]^+$ cations also reflect the presence of close Al atoms able to accommodate hexaaqua complexes of Co^{II}, but not bare Co^{II}. The bare Co^{II} species are preferentially formed in the lowest cobalt loading in dehydrated zeolites whereas Co–oxo species are created only after saturation of the cationic sites for divalent cations created by aluminum pairs (i.e., Al-O-(Si-O)$_2$-Al sequences) in one ring. This behavior results in a plateau in the dependence of the adsorbed [D_3]acetonitrile upon cobalt loading. Co–oxo species, which do not adsorb [D_3]acetonitrile, are absent in the Co-TNU-9 sample, as evidenced by 1) the linear increase in the amount of adsorbed CD_3CN with cobalt loading and 2) the same concentration of cobalt species exchanged in the zeolite and bare Co^{II}. Therefore, only isolated single aluminum atoms and aluminum pairs of Al-O-(Si-O)$_2$-Al sequences are present in the TNU-9 sample. Their resulting concentrations are given in Table 6.

Table 6. Aluminum distribution and the concentration of cationic sites in the TNU-9 zeolite.

Al single [%]	Al pairs [%]	Al pair in the α site [%]	Al pair in the β site [%]	Al pair in the γ site [%]
40	60	9	51	< 1

Siting of divalent cations and aluminum pairs

Zeolite rings with aluminum pairs (i.e., Al-O-(Si-O)$_2$-Al sequences) that are able to accommodate bare Co^{II} represent general cationic sites for bare divalent cations. Therefore, the siting of Al-O-(Si-O)$_2$-Al sequences and bare Co^{II} in the zeolite rings will be discussed together. Zeolite frameworks are relatively rigid and allow only limited structural rearrangements of the local structure of the cationic sites upon binding of Co^{II}[3a, 3b] (or other Me^{II}[3a, 31]) depending on the framework type and the character of the cationic site. The visible spectrum of Co^{II} reflects their coordination and represents a fingerprint of the cationic site accommodating this cation. This fingerprint, in combination with a visual inspection of the structure of the zeolite framework, can be employed to suggest cationic sites of bare Co^{II}.

Visible spectroscopy of bare Co^{II} as a probe was successfully applied to analyze the cationic sites of Co^{II} for ZSM-5,[5c] the β-zeolite,[30d] and ferrierite[5b] for which the sites were later confirmed by synchrotron powder XRD.[22] Analysis of the Co^{II} d–d transition in the visible region evidences the presence of three spectroscopic species in the dehydrated Co,Na-TNU-9/a–e samples, reflecting three types of bare Co^{II} located in three cationic sites designated as the α, β, and γ sites and corresponding to a single band, a quartet, and a doublet, respectively, in the spectrum (Table 4). The wavenumbers of the d–d transitions of Co^{II} in the individual sites of the Co,Na-TNU-9/a–e samples (Table 4) are compared with those already reported for Co^{II} in the MFI, FER, and MOR structures. The significant similarity between the spectra of Co^{II} in the TNU-9 zeolite and in the other pentasil zeolites allows the assignment of the bands to the cationic sites described in the section Possible cationic sites in TNU-9. Conversely, spectroscopic species typical of aluminum-rich zeolites (e.g., a doublet at around 25 000 cm^{-1} reflecting planar-trigonal Co^{II} in the LTA structure) are missing.[47]

The concurrent occupation of both the α and β sites by Co^{II} in the Co,Na-TNU-9/a–e samples does not provide a reliable set of linearly independent equations describing the relation between the cobalt loading in the zeolite and the intensities of the individual spectroscopic species. Therefore, the concentration of Co^{II} in the individual sites in the fully loaded Co-TNU-9/e sample (i.e., the concentration of Al-O-(Si-O)$_2$-Al sequences in the rings of the α, β, and γ sites) can be only roughly estimated by using the ratio of the extinction coefficients of Co^{II} located in the α and β sites in the MFI, FER, and MOR structures. In this way, we estimated the concentrations of Co^{II} in the α, β, and γ sites to be 15–30, 70–85, and < 1 %, respectively.

Analysis of the positions and relative intensities of the bands of the antisymmetric T-O-T stretching lattice vibrations of zeolite rings accommodating bare Co^{II} obtained from the FTIR spectra of dehydrated zeolites is another completely independent method for the analysis of the Co^{II} siting and the siting of Al-O-(Si-O)$_2$-Al sequences.[30] The coordination of bare Co^{II} to skeletal oxygen atoms of one ring causes a perturbation of the framework T-O-T vibrations resulting in the appearance of new bands in the FTIR spectrum. Their wavenumbers are characteristic of the individual cationic sites. Analysis of the FTIR spectra of the dehydrated Co,Na-TNU-9/a–e samples reveals the presence of only two new bands corresponding to two different rings accommodating Co^{II}. Their intensities increase linearly with the cobalt loading in the zeolite in excellent agreement with the results of visible spectroscopy. The concentration of Co^{II} in the γ site is negligible and these Co^{II} are not reflected in the FTIR spectrum.

FTIR spectroscopy of antisymmetric T-O-T stretching lattice vibrations, in contrast to the visible spectroscopy of Co^{II} d–d transitions, allows the estimation of the concentration of Co^{II} in the α and β sites. Previous results for ferrierite showed[30b] that the extinction coefficients of T-O-T stretching antisymmetric vibration of the rings accommodating Co^{II} in the α and β sites do not differ. Based on these results we estimate that the Co^{II} in the α and β sites represent 15 and 85 %, respectively, of all the Co^{II} in the fully exchanged Co,Na-TNU-9/e. By analogy, the results also mean that 9 and 51 % (Table 6) of all the aluminum atoms (i.e., Al_{total}) form the α and β cationic sites, respectively. The β site represents the main extra-framework position for divalent cations in the TNU-9 zeolite. The aluminum atoms of the Al-O-(Si-O)$_2$-Al sequences of the 6-ring forming the β site correspond to the major fraction of the aluminum atoms in the TUN framework.

There is only one structure of the α site in the TUN framework with two possible aluminum sitings in the 6-ring that are indistinguishable by FTIR and visible spectroscopy. The only way to distinguish the aluminum sitings in the 6-ring is by determination of the aluminum siting. However, this is beyond the scope of this study due to the high number of framework T sites and the possible effects of the presence of next-next-nearest aluminum neighbors on the ^{27}Al isotropic chemical shifts of aluminum atoms in Al-O-(Si-O)$_2$-Al sequences. The α site is located on the TUN straight channel wall (Figure 1) and it connects two channel intersections. The cation at this site is placed in the 6-ring plane and thus exhibits an open coordination sphere and is easily accessible only from the straight channel. Each of the two aluminum atoms of the Al-O-(Si-O)$_2$-Al sequences forming the α site is located at the opposite channel intersection for both the possible aluminum sitings (T4 and T24 or T10 and T22). Most likely, the two corresponding Brønsted acid sites are placed in the same way. The location and arrangement of the α site are very similar to those in the ZSM-5 zeolite.

Conversely, there are six distinct 6-rings attributable to the topology of the β cationic site. These are schematically depicted in Figures 3–5. The high number of 6-rings that can potentially form the β cationic site represents a high uncertainty in

the analysis of the siting of bare divalent cations and Al-O-(Si-O)$_2$-Al sequences creating the β cationic site. Therefore, a new approach involving the use of not only visible spectroscopy of Co^{II} d–d transitions and FTIR spectroscopy of antisymmetric T-O-T stretching lattice vibrations, but also extensive periodic DFT calculations, including molecular dynamics, and ^{27}Al 3Q MAS NMR spectroscopy has been developed and presented. Analysis of the ^{27}Al 3Q MAS NMR spectra (Table 3) showed that the maximum concentration of one of the aluminum coordinations (T site) is 40% of all the aluminum atoms (i.e., Al_{total}); 85% of aluminum pairs, that is, 51% of all the aluminum atoms (Table 6), create the β cationic sites. Therefore, these aluminum pairs cannot contain two aluminum atoms with the same ^{27}Al isotropic chemical shift (i.e., the two aluminum atoms of the Al_{pair} cannot be located in the same crystallographically distinguishable framework T site). This finding permits the exclusion of the $\beta_{T5T2T22}$ and β_{T9T6T4} sites with all the possible aluminum sitings in the T5-T2-T22-T5-T2-T22 and T9-T6-T4-T9-T6-T4 rings, respectively, forming these sites (Table 2). The Al-O-(Si-O)$_2$-Al sequences located in these two 6-rings must have both the aluminum atoms accommodated in the same crystallographically distinguishable framework T site. Conversely, the Al-O-(Si-O)$_2$-Al sequences present in the other three 6-rings forming possible β sites (T11-T4-T9-T9-T4-T11, T8-T10-T11-T11-T10-T8, and T14-T12-T21-T21-T12-T14) have both the aluminum atoms in either different or the same crystallographically distinguishable framework T sites. Only the latter are excluded. Therefore, the $\beta_{T11T4T9}$, $\beta_{T8T10T11}$, and $\beta_{T14T12T21}$ sites with the aluminum sitings of both the aluminum atoms in T4, T10, and T12, respectively, are ruled out (Table 2). The $\beta_{T23T19T17}$ site formed by the T23-T19-T17-T21-T12-T14 ring has three possible aluminum sitings of both the aluminum atoms located in different crystallographically distinguishable framework T sites. Therefore, subsequent optimizations of the two models of the α site and only the six models of the β sites (Tables 2 and 5) were carried out.

Although in general the relative binding energies of Co^{II} in various possible cationic sites cannot be employed to suggest the siting of Co^{II}, comparison of the relative binding energies with the experimental data regarding the preference in the occupation of the α and β cationic sites can provide useful information concerning the cobalt siting in the TNU-9 zeolite. Therefore, the relative binding energies of Co^{II} calculated for the eight computational models (Table 5) can serve to select the probable 6-rings forming the β cationic site. Both the visible and FTIR experiments revealed that there is no preference in the occupation of the α and β cationic sites because the intensities of Co^{II} located in the α and β sites concurrently increase with increasing cobalt loading. This finding indicates that the relative binding energies of Co^{II} should be similar for both the α and β cationic sites. The relative binding energy of Co^{II} in the α site is 12–16 kcal mol^{-1} (Table 5) and only three computational models of the β cationic site yield similar values: $\beta_{T11T4T9}$(T11T9) 13 kcal mol^{-1}, $\beta_{T14T12T21}$(T14T21) 15 kcal mol^{-1}, and $\beta_{T8T10T11}$(T11T8) 18 kcal mol^{-1} (Table 5). Because the DFT-calculated coordination of Me^{II} in the β cation sites of zeolites with the FER[3a,31] and *BEA[3b] structures is near-planar (Figure 17), we suggest based on the results of visible spectroscopy of the Co^{II} d–d transitions (Table 4) that the near-planar $\beta_{T11T4T9}$ site (Table 5 and Figures 14 and 17) located at the channel intersection (Figure 1) with the two aluminum atoms accommodated in T11 and T9 is the best candidate for the observed β cationic site.

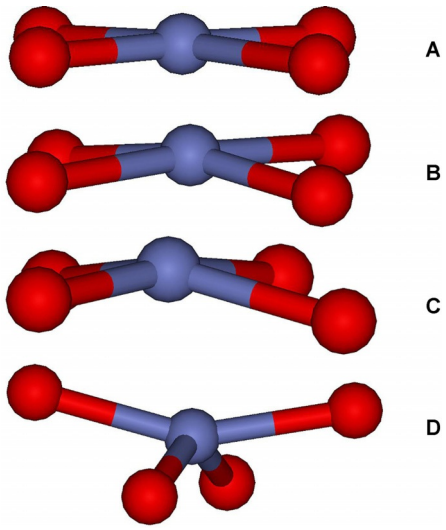

Figure 17. Optimized structures of the CoO_4 moiety of A) the β-2 model of Co-ferrierite,[3a] B) the $\beta_{T11T4T9}$(T11T9) model of Co-TNU-9, C) the $\beta_{T8T10T11}$(T11T8) model of Co-TNU-9, and D) the $\beta_{T14T12T21}$(T14T21) model of Co-TNU-9 (D). Cobalt atoms are in blue and oxygen atoms in red.

The near-planar $\beta_{T8T10T11}$ site (Table 5 and Figures 14 and 17) present also at the channel intersection (Figure 1) with the two aluminum atoms placed in T11 and T8 is another less likely candidate. The site has one elongated Co–O_{Si} bond (O of SiO_4; Table 5 and Figure 14). Conversely, the $\beta_{T14T12T21}$ site (Table 5 and Figures 15 and 17) with the two aluminum atoms in T14 and T21 can be ruled out because the site possesses a Co^{II} coordination that is deformed tetrahedral rather than near-planar (Figure 17). It should be noted that a change in the symmetry of the cation is reflected in a significant change in the d–d spectrum.[48] The divalent cations accommodated in the $\beta_{T11T4T9}$ and $\beta_{T8T10T11}$ sites as well as the corresponding aluminum atoms forming these cationic sites (and most likely also the corresponding Brønsted acid sites) are present at the channel intersection. The location of the $\beta_{T11T4T9}$ and $\beta_{T8T10T11}$ sites in the TUN framework is therefore very similar to that of the β site in the MFI framework.

The above-demonstrated newly developed approach to determining the siting of bare divalent cations significantly reduced the number of 6-rings as possible candidates forming cationic sites. Furthermore, ^{27}Al 3Q MAS NMR spectroscopy further lowered the number of 6-rings with various aluminum sitings from 15 to 6 (β cationic site), and moreover, the DFT calculations further limited the number of 6-ring candidates to one best structure ($\beta_{T11T4T9}$ site with the two aluminum atoms accommodated in T11 and T9) and one less likely structure. The selection of a highly probable 6-ring candidate creating the cationic site from a high number of 6-rings together with

the estimation of the aluminum siting in the corresponding 6-ring candidate represent significant progress in the analysis of cation siting in silicon-rich zeolites compared with the approach based on an empirical interpretation of the visible spectra.[5,30d]

The bands at 22400 and 23000 cm^{-1} (Table 4) reflect Co^{II} with pseudo-octahedral coordination. This coordination was suggested for Co^{II} siting in the hexagonal prism of the so-called "boat-shape" site in MOR, FER, and MFI structures. However, hexagonal prisms are not present in the TUN framework. Therefore, the γ site is suggested to reflect Co^{II} located in "boat-shape" sites (e.g., formed by the T13-T20-T16-T1-T23-T21-T7-T15 and T2-T22-T18 atoms). The exact aluminum siting of the two aluminum atoms in the γ site is not known. However, the Co^{II} concentration in the γ site of the maximum Co^{II}-loaded Co,Na-TNU-9/e sample is negligible (<1% of Co^{II}) and thus also the concentration of the corresponding aluminum pairs. Moreover, Me^{II} species in this site with pseudo-octahedral coordination exhibit a fully occupied coordination sphere and thus their possible activity as catalytic and sorption centers is very limited.

Siting of aluminum atoms in framework T sites

Because there are 24 crystallographically distinguishable framework T sites in the TUN framework, our ability to determine the aluminum siting is significantly limited. Nevertheless, some conclusions regarding the aluminum siting in the individual T sites of the TUN framework can be drawn from the results of this study. Thus, 51% of all the aluminum atoms (Table 6) form the β cationic site and the aluminum atoms of the corresponding Al-O-(Si-O)$_2$-Al sequence creating this site occupy most likely the T9 and T11 framework sites (ca. 26% each). In addition, isolated single aluminum atoms are likely also located in these T sites, because the relative concentrations of the aluminum atoms corresponding to the individual resonances are 30–40%. However, there is another possibility that isolated single aluminum atoms accommodated in other crystallographically distinguishable framework T sites (i.e., neither T9 nor T11) exhibit indistinguishable ^{27}Al isotropic chemical shifts.

The aluminum atoms of aluminum pairs creating the α cationic site are located at either the T4 and T24 or T10 and T22 sites. They form a minor fraction (5% each) of all the aluminum atoms. The α site either corresponds to two ^{27}Al NMR resonances (5%) or, due to a random degeneracy of ^{27}Al NMR parameters, it is reflected only in one ^{27}Al NMR resonance (10%).

Concerning the siting of isolated single aluminum atoms, we can only estimate the number of T sites occupied by aluminum atoms. Analysis of the ^{27}Al 3Q MAS NMR spectra of the TNU-9 sample reveals the presence of three ^{27}Al NMR resonances (Table 3). Because the aluminum relative concentrations are 30–40% (Table 3), there are at least two isolated single aluminum atoms. Based on the calculated pattern of the ^{27}Al isotropic chemical shifts of the 24 T sites in ZSM-5, there should be no more than around five isolated single aluminum atoms in the TNU-9 sample.[21]

The location of the framework aluminum atoms and thus of the positively charged active species (mainly protons) compensating them is of great importance. The aluminum in zeolites with similar size channels as TNU-9 and ZSM-5 can be located in either the channels (with a limited reaction volume) or at the channel intersections (with a large reaction volume). Our analysis of the siting of Al-O-(Si-O)$_2$-Al sequences in the TNU-9 sample revealed that at least 60% of all the aluminum atoms are located at the channel intersections. This result is very similar to those obtained for the ZSM-5 zeolites synthesized by using the tetrapropylammonum cation as the structure directing agent.[4]

Co^{II} siting and aluminum organization in TNU-9 and other pentasil zeolites and their relevance for catalysis

The siting of bare Co^{II} and thus of other divalent cations and the siting of aluminum pairs in the TNU-9 zeolite are similar to those already reported for pentasil zeolites with high concentrations of aluminum pairs (more than 50% of all the aluminum atoms). The α site of two 5-rings composing one 6-ring is highly similar to those of zeolites with the MOR, FER, MFI, and *BEA topologies. The β site representing the near-planar 6-ring is similar to those of zeolites with the FER, MFI, and *BEA structures, whereas the β site in the MOR framework created by a twisted 8-ring can be regarded as the exception in pentasil zeolites. The boat-shape γ site exhibits a topology highly similar to those of the MOR and FER structures. There is also a significant similarity between the TNU-9 and pentasil zeolites concerning the population of aluminum pairs and the cationic sites. The β site is dominant in the TNU-9 zeolite and represents 85% of aluminum pairs and thus the sites for divalent cations. The concentration of the α site (15% of aluminum pairs) fits well with the values well known for other pentasil zeolites (12–30% of aluminum pairs). The only difference between the TNU-9 and pentasil zeolites is the negligible concentration (<1% of aluminum pairs) of the γ site. This site represents 5–10% of aluminum pairs in the zeolites with MOR, FER, MFI, and *BEA structures.

Access to the β site is controlled by 8-rings in the MOR and FER topologies and only the α site exhibits unrestricted access in these matrices because it is located in the straight channel. The β site in the *BEA structure is analogously located at the intersection of the *BEA channels, whereas the α site in the *BEA structure is inaccessible because it is placed inside the β cage. Access to the cation accommodated in the latter site is restricted by a 6-ring. Therefore, the sitings of aluminum pairs and divalent cations in the TNU-9 zeolite resemble the most those of the ZSM-5 zeolite. The TNU-9 zeolite can be thus regarded as an analogue of the ZSM-5 zeolite.

Concerning the concentration of aluminum pairs, the ion-exchange capacity for divalent complexes, and the ability to accommodate bare divalent cations, the TNU-9 zeolite (60% of aluminum pairs, Si/Al 14) can be regarded as an analogue of commercial ZSM-5, mordenite, and ferrierite, which exhibit 60–70% of aluminum pairs (Si/Al: ZSM-5 14–30, mordenite and ferrierite 8.5–10). The aluminum distribution in ZSM-5 zeolites

is well known to significantly vary with the synthesis conditions. ZSM-5 zeolites with either more than 85% of aluminum atoms in aluminum pairs or with 90% of isolated single aluminum atoms have already been reported for a wide ratio of Si/Al (12–40).[49] Conversely, the concentrations of isolated single aluminum atoms and aluminum pairs in Al-O-(Si-O)$_2$-Al sequences in the TNU-9 zeolite reach average values guaranteeing the catalytic activity of TNU-9-based materials for both reactions requiring the presence of isolated single aluminum atoms as well as those demanding aluminum pairs. It should be stressed that tuning the aluminum distribution in the TUN framework opens a window of possibilities for improving catalysts based on TNU-9 by optimizing the concentrations of isolated single aluminum atoms and aluminum pairs for individual reactions.

Conclusions

The aluminum distribution in the TUN framework of the TNU-9 zeolite has been determined and the locations of the aluminum pairs forming the corresponding α and β cationic sites for bare divalent cations have been suggested. Because the TNU-9 matrix is one of the most complex zeolites known, possessing 24 crystallographically distinguishable framework T sites and a highly complicated channel structure, the standard approach based on the application of bare Co^{II} monitored by FTIR and visible spectroscopy was insufficient. Therefore, we have developed a new significantly improved procedure that includes in addition to the standard methods also ^{27}Al 3Q MAS NMR spectroscopy and extensive periodic DFT calculations, including molecular dynamics. This multi-spectroscopic and theoretical approach was shown to be a very powerful tool for analyzing the siting of aluminum pairs and divalent cations in the TNU-9 zeolite.

Our results reveal that 40 and 60% of aluminum atoms in the TUN framework are isolated single aluminum atoms and aluminum pairs (i.e., Al-O-(Si-O)$_2$-Al sequences in one 6-ring forming cationic sites for divalent cations), respectively. Moreover, there are no Al-O-Si-O-Al sequences in the TUN framework. Both types of aluminum arrangements, that is, isolated single aluminum atoms and aluminum pairs, are important for the catalytic properties of the prepared materials. The isolated single aluminum atoms are able to accommodate exclusively monovalent cationic species whereas aluminum pairs can stabilize divalent cations and divalent species. In addition, aluminum pairs can create two close and co-operating monovalent centers. The concentrations of isolated single aluminum atoms and aluminum pairs are similar to those of commercial ZSM-5 zeolites with a Si/Al ratio of 12–30 and commercial ferrierites and mordenites with a Si/Al ratio of around 9. The concentrations are far from the extreme values obtained for some ZSM-5 zeolites (either $>$85% of aluminum pairs or 90% of isolated single aluminum atoms). This result indicates that TNU-9-based catalysts should be active in both reactions requiring isolated single aluminum atoms as well as those demanding the presence of aluminum pairs and that there is enough room for improvement by tuning the aluminum distribution to reach optimum values for specific reactions.

Our study shows that Al-O-(Si-O)$_2$-Al sequences are predominantly present in two types of six-membered rings forming the corresponding α and β cationic sites for bare divalent cations. The α site represents the 6-ring formed from two 5-rings and is located on the TUN straight channel wall and connects two channel intersections. The two aluminum atoms are placed in positions diagonally across the 6-ring occupying either T4 and T24 or T10 and T22. The Co^{II} is placed in the plane of the 6-ring and is coordinated to four oxygens of two AlO_4^- tetrahedra and one oxygen of a SiO_4 tetrahedron. The Co^{II} exhibits an open coordination sphere and is easily accessible only from the straight channel; 9% of aluminum atoms (15% of aluminum pairs) are present in this site.

The β site is the main site for divalent cations and it accommodates at least 51% of aluminum atoms (85% of aluminum pairs). The near-planar $\beta_{T11T4T9}$ site located at the channel intersection with the two aluminum atoms accommodated in T11 and T9 is the best candidate for the observed β cationic site. The Co^{II} is placed in the plane of this ring and is coordinated to four oxygen atoms of two AlO_4^- tetrahedra. The Co^{II} accommodated in the β site are present at the channel intersections.

Based on the siting of Al-O-(Si-O)$_2$-Al sequences in the TNU-9 sample, our study has revealed that at least 60% of all the aluminum atoms (and most likely also the corresponding Brønsted acid sites) are located at the channel intersections. The location of aluminum pairs and thus of bare divalent cations in the TUN framework is very similar to that in MFI.

Acknowledgements

This work was supported by the Grant Agency of the Czech Republic under Project No. 15-14007S and the RVO 61388955. For zeolite synthesis, the authors acknowledge the assistance provided by the Research Infrastructure NanoEnviCz, supported by the Ministry of Education, Youth and Sports of the Czech Republic under Project No. LM2015073. This work was supported by The Ministry of Education, Youth and Sports from the Large Infrastructures for Research, Experimental Development and Innovations project "IT4Innovations National Supercomputing Center–LM2015070".

Conflict of interest

The authors declare no conflict of interest.

Keywords: aluminum · cobalt · density functional calculations · structure elucidation · zeolites

[1] http://www.iza-structure.org/databases.
[2] J. Dědeček, Z. Sobalik, B. Wichterlova, *Catal. Rev. Sci. Eng.* **2012**, *54*, 135–223.
[3] a) S. Sklenak, P. C. Andrikopoulos, S. R. Whittleton, H. Jirglova, P. Sazama, L. Benco, T. Bucko, J. Hafner, Z. Sobalik, *J. Phys. Chem. C* **2013**, *117*, 3958–3968; b) P. Sazama, E. Tabor, P. Klein, B. Wichterlova, S. Sklenak, L. Mokrzycki, V. Pashkkova, M. Ogura, J. Dedecek, *J. Catal.* **2016**, *333*, 102–114; c) P. Klein, V. Pashkova, H. M. Thomas, S. R. Whittleton, J. Brus, L.

Kobera, J. Dedecek, S. Sklenak, *J. Phys. Chem. C* **2016**, *120*, 14216 – 14225.
[4] V. Pashkova, S. Sklenak, P. Klein, M. Urbanova, J. Dedecek, *Chem. Eur. J.* **2016**, *22*, 3937 – 3941.
[5] a) J. Dědeček, B. Wichterlova, *J. Phys. Chem. B* **1999**, *103*, 1462 – 1476; b) D. Kaucký, J. I. Dedecek, B. Wichterlova, *Microporous Mesoporous Mater.* **1999**, *31*, 75 – 87; c) J. Dědeček, D. Kaucky, B. Wichterlova, *Microporous Mesoporous Mater.* **2000**, *35 – 6*, 483 – 494.
[6] a) J. Dědeček, D. Kaucky, B. Wichterlova, *Chem. Commun.* **2001**, 970 – 971; b) J. Dědeček, D. Kaucky, B. Wichterlova, O. Gonsiorova, *Phys. Chem. Chem. Phys.* **2002**, *4*, 5406 – 5413; c) V. Gábová, J. Dedecek, J. Cejka, *Chem. Commun.* **2003**, 1196 – 1197; d) Z. Sobalik, P. Sazama, J. Dedecek, B. Wichterlova, *Appl. Catal. A* **2014**, *474*, 178 – 185; e) S. Sklenak, J. Dedecek, C. Li, F. Gao, B. Jansang, B. Boekfa, B. Wichterlova, J. Sauer, *Collect. Czech. Chem. Commun.* **2008**, *73*, 909 – 920.
[7] a) J. Dědeček, B. Wichterlova, *Phys. Chem. Chem. Phys.* **1999**, *1*, 629 – 637; b) J. Dědeček, L. Capek, B. Wichterlova, *Appl. Catal. A* **2006**, *307*, 156 – 164.
[8] J. Li, A. Corma, J. Yu, *Chem. Soc. Rev.* **2015**, *44*, 7112 – 7127.
[9] a) F. Gramm, C. Baerlocher, L. B. McCusker, S. J. Warrender, P. A. Wright, B. Han, S. B. Hong, Z. Liu, T. Ohsuna, O. Terasaki, *Nature* **2006**, *444*, 79 – 81; b) S. B. Hong, H.-K. Min, C.-H. Shin, P. A. Cox, S. J. Warrender, P. A. Wright, *J. Am. Chem. Soc.* **2007**, *129*, 10870 – 10885.
[10] H. K. Min, S. B. Hong, *J. Phys. Chem. C* **2011**, *115*, 16124 – 16133.
[11] F. Bleken, W. Skistad, K. Barbera, M. Kustova, S. Bordiga, P. Beato, K. P. Lillerud, S. Svelle, U. Olsbye, *Phys. Chem. Chem. Phys.* **2011**, *13*, 2539 – 2549.
[12] M. T. Portilla, F. J. Llopis, C. Martinez, S. Valencia, A. Corma, *Appl. Catal. A* **2011**, *393*, 257 – 268.
[13] H. K. Min, S. H. Cha, S. B. Hong, *ACS Catal.* **2012**, *2*, 971 – 981.
[14] N. Danilina, E. L. Payrer, J. A. van Bokhoven, *Chem. Commun.* **2010**, *46*, 1509 – 1510.
[15] C. Y. Chen, X. Ouyang, S. I. Zones, S. A. Banach, S. A. Elomari, T. M. Davis, A. F. Ojo, *Microporous Mesoporous Mater.* **2012**, *164*, 71 – 81.
[16] W. Xu, S. J. Miller, P. K. Agrawal, C. W. Jones, *Appl. Catal. A* **2013**, *459*, 114 – 120.
[17] Y. Byun, S. H. Cha, H. J. Jeon, S. B. Hong, *J. Phys. Chem. C* **2016**, *120*, 6125 – 6135.
[18] S. H. Cha, K. Lee, Y. Byun, S. B. Hong, *J. Phys. Chem. C* **2016**, *120*, 11552 – 11560.
[19] C. Franch-Martí, C. Alonso-Escobar, J. L. Jorda, I. Peral, J. Hernandez-Fenollosa, A. Corma, A. E. Palomares, F. Rey, G. Guilera, *J. Catal.* **2012**, *295*, 22 – 30.
[20] M. Moreno-González, T. Blasco, K. Gora-Marek, A. E. Palomares, A. Corma, *Catal. Today* **2014**, *227*, 123 – 129.
[21] a) S. Sklenak, J. Dedecek, C. Li, B. Wichterlova, V. Gabova, M. Sierka, J. Sauer, *Angew. Chem. Int. Ed.* **2007**, *46*, 7286 – 7289; *Angew. Chem.* **2007**, *119*, 7424 – 7427; b) S. Sklenak, J. Dedecek, C. Li, B. Wichterlova, V. Gabova, M. Sierka, J. Sauer, *Phys. Chem. Chem. Phys.* **2009**, *11*, 1237 – 1247.
[22] a) M. C. Dalconi, G. Cruciani, A. Alberti, P. Ciambelli, M. T. Rapacciuolo, *Microporous Mesoporous Mater.* **2000**, *39*, 423 – 430; b) M. C. Dalconi, A. Alberti, G. Cruciani, P. Ciambelli, E. Fonda, *Microporous Mesoporous Mater.* **2003**, *62*, 191 – 200; c) M. C. Dalconi, A. Alberti, G. Cruciani, *J. Phys. Chem. B* **2003**, *107*, 12973 – 12980.
[23] a) W. J. Mortier, J. J. Pluth, J. V. Smith, *Mater. Res. Bull.* **1975**, *10*, 1037 – 1045; b) W. J. Mortier, *J. Phys. Chem.* **1977**, *81*, 1334 – 1338; c) J. L. Schlenker, J. J. Pluth, J. V. Smith, *Mater. Res. Bull.* **1978**, *13*, 169 – 174.
[24] D. Massiot, F. Fayon, M. Capron, I. King, S. Le Calve, B. Alonso, J. O. Durand, B. Bujoli, Z. H. Gan, G. Hoatson, *Magn. Reson. Chem.* **2002**, *40*, 70 – 76.
[25] G. Engelhardt, U. Lohse, E. Lippmaa, M. Tarmak, M. Magi, *Z. Anorg. Allg. Chem.* **1981**, *482*, 49 – 64.
[26] J. Dedecek, M. J. Lucero, C. B. Li, F. Gao, P. Klein, M. Urbanova, Z. Tvaruzkova, P. Sazama, S. Sklenak, *J. Phys. Chem. C* **2011**, *115*, 11056 – 11064.
[27] J. A. van Bokhoven, D. C. Koningsberger, P. Kunkeler, H. van Bekkum, A. P. M. Kentgens, *J. Am. Chem. Soc.* **2000**, *122*, 12842 – 12847.
[28] P. Sarv, C. Fernandez, J. P. Amoureux, K. Keskinen, *J. Phys. Chem.* **1996**, *100*, 19223 – 19226.
[29] L. B. Alemany, *Appl. Magn. Reson.* **1993**, *4*, 179 – 201.
[30] a) Z. Sobalík, Z. Tvaruzkova, B. Wichterlova, *J. Phys. Chem. B* **1998**, *102*, 1077 – 1085; b) Z. Sobalík, Z. Tvaruzkova, B. Wichterlova, *Microporous Mesoporous Mater.* **1998**, *25*, 225 – 228; c) J. E. Šponer, Z. Sobalik, J. Leszczynski, B. Wichterlova, *J. Phys. Chem. B* **2001**, *105*, 8285 – 8290; d) J. Dedecek, L. Capek, D. Kaucky, Z. Sobalik, B. Wichterlova, *J. Catal.* **2002**, *211*, 198 – 207.
[31] S. Sklenak, P. C. Andrikopoulos, B. Boekfa, B. Jansang, J. Novakova, L. Benco, T. Bucko, J. Hafner, J. Dedecek, Z. Sobalik, *J. Catal.* **2010**, *272*, 262 – 274.
[32] a) T. Takaishi, M. Kato, K. Itabashi, *J. Phys. Chem.* **1994**, *98*, 5742 – 5743; b) T. Takaishi, M. Kato, K. Itabashi, *Zeolites* **1995**, *15*, 21 – 32.
[33] a) G. Kresse, J. Hafner, *Phys. Rev. B* **1993**, *48*, 13115 – 13118; b) G. Kresse, J. Hafner, *Phys. Rev. B* **1994**, *49*, 14251 – 14269; c) G. Kresse, J. Furthmuller, *Comput. Mater. Sci.* **1996**, *6*, 15 – 50; d) G. Kresse, J. Furthmuller, *Phys. Rev. B* **1996**, *54*, 11169 – 11186.
[34] P. E. Blöchl, *Phys. Rev. B* **1994**, *50*, 17953 – 17979.
[35] G. Kresse, D. Joubert, *Phys. Rev. B* **1999**, *59*, 1758 – 1775.
[36] a) J. P. Perdew, Y. Wang, *Phys. Rev. B* **1992**, *45*, 13244 – 13249; b) J. P. Perdew, J. A. Chevary, S. H. Vosko, K. A. Jackson, M. R. Pederson, D. J. Singh, C. Fiolhais, *Phys. Rev. B* **1992**, *46*, 6671 – 6687.
[37] S. Nosé, *J. Chem. Phys.* **1984**, *81*, 511 – 519.
[38] a) L. Verlet, *Phys. Rev.* **1967**, *159*, 98 – 103; b) L. Verlet, *Phys. Rev.* **1968**, *165*, 201 – 214.
[39] P. Klein, J. Dedecek, H. M. Thomas, S. R. Whittleton, V. Pashkova, J. Brus, L. Kobera, S. Sklenak, *Chem. Commun.* **2015**, *51*, 8962 – 8965.
[40] a) K. J. D. MacKenzie, M. E. Smith, *Multinuclear Solid-State NMR of Inorganic Materials*, Pergamon, Oxford, **2002**; b) J. Dědeček, S. Sklenak, C. Li, F. Gao, J. Brus, Q. Zhu, T. Tatsumi, *J. Phys. Chem. C* **2009**, *113*, 14454 – 14466.
[41] J. Dědeček, S. Sklenak, C. Li, B. Wichterlova, V. Gabova, J. Brus, M. Sierka, J. Sauer, *J. Phys. Chem. C* **2009**, *113*, 1447 – 1458.
[42] a) D. Kaucký, J. Dědeček, A. Vondrova, Z. Sobalik, B. Wichterlova, *Collect. Czech. Chem. Commun.* **1998**, *63*, 1781 – 1792; b) O. Bortnovsky, Z. Sobalik, B. Wichterlova, *Microporous Mesoporous Mater.* **2001**, *46*, 265 – 275.
[43] Z. Sobalik, J. Dedecek, D. Kaucky, B. Wichterlova, L. Drozdova, R. Prins, *J. Catal.* **2000**, *194*, 330 – 342.
[44] L. Benco, T. Bucko, R. Grybos, J. Hafner, Z. Sobalik, J. Dedecek, J. Hrusak, *J. Phys. Chem. C* **2007**, *111*, 586 – 595.
[45] a) L. Čapek, J. Dedecek, B. Wichterlova, *J. Catal.* **2004**, *227*, 352 – 366; b) L. Čapek, J. Dedecek, P. Sazama, B. Wichterlova, *J. Catal.* **2010**, *272*, 44 – 54.
[46] P. Sazama, L. Mokrzycki, B. Wichterlova, A. Vondrova, R. Pilar, J. Dedecek, S. Sklenak, E. Tabor, *J. Catal.* **2015**, *332*, 201 – 211.
[47] a) K. Klier, *J. Am. Chem. Soc.* **1969**, *91*, 5392; b) K. Klier, R. Kellerman, P. J. Hutta, *J. Chem. Phys.* **1974**, *61*, 4224 – 4234.
[48] A. B. P. Lever, *Inorganic Electronic Spectroscopy*, 2nd ed., Elsevier, Amsterdam, **1984**, pp. 479 – 505.
[49] a) J. Dedecek, V. Balgova, V. Pashkova, P. Klein, B. Wichterlova, *Chem. Mater.* **2012**, *24*, 3231 – 3239; b) V. Pashkova, P. Klein, J. Dedecek, V. Tokarova, B. Wichterlova, *Microporous Mesoporous Mater.* **2015**, *202*, 138 – 146.

Manuscript received: December 5, 2016
Accepted manuscript online: March 8, 2017
Version of record online: April 25, 2017

